Supporting Information

Regulating Ru Active Sites by Pd alloying to Significantly Enhance Hydrazine Oxidation for Energy-saving Hydrogen Production

Simeng Zhao [a], Yankai Zhang [a], Haibo Li [a], Suyuan Zeng [a], Rui Li [a], Qingxia Yao [a], Hongyan Chen [a], Yao Zheng [b,*], Konggang Qu [a,*]

[a] School of Chemistry and Chemical Engineering, Shandong Provincial Key Laboratory/Collaborative Innovation Center of Chemical Energy Storage & Novel Cell Technology, Liaocheng University, Liaocheng 252059, China

[b] School of Chemical Engineering and Advanced Materials, The University of Adelaide, Adelaide, SA 5005, Australia

Email: qukonggang@lcu.edu.cn; yao.zheng01@adelaide.edu.au

Experimental section

1. Chemical and materials

$RuCl_3$ was purchased from Shanghai Aladdin Industrial Corporation. K_2PdCl_4 was purchased from Shanghai Energy Chemical. The commercial 20% Pt/C and carbon black (Cabot Vulcan XC-72R) were provided by Shanghai Hesen Corporation. The 5% Nafion solution and Nafion 115 membrane were provided by Sigma-Aldrich Corporation.

2. The optimization of the molar ratio of Ru and Pd

The optimization of different molar ratio of Ru and Pd (5:5, 7:3, 8:2 and 9:1) during sample preparation was performed in advance. Additionally, the regulation of the composition ratio allowed us to select the most active element ratio. The effect of different molar ration of Ru and Pd on electrocatalytic performances of HER and HzOR has been examined, which shows the sample obtained with 8:2 molar ratio of Ru and Pd has the best HER and HzOR activity, thus we mainly focused on the discussion about the RuPd alloy on activated carbon with 8:2 molar ratio of Ru and Pd in the manuscript.

3. Physical characterizations

The morphology and structure were examined by the transmission electron microscope (TEM, Talos F200X G2), powder X-ray diffraction (XRD, SmartLab 9kW) and Raman spectrometer with an excitation wavelength of 532 nm (HORIBA iHR550). The high-resolution TEM and HAADF-STEM were recorded by JEM-ARM300F TEM/STEM with a spherical aberration corrector working at 300 kV. The componential information was obtained by TEM energy-dispersive X-ray spectroscopy (EDS) mapping, X-ray photoelectron spectroscopy (XPS, Kratos Axis Ultra spectrometer). The specific surface areas were extracted with nitrogen adsorption-desorption isotherm (Micrometrics 2460) by the Brunauer-Emmett-Teller (BET) model at a pressure range of P/P_0 = 0.05-0.3, along with the Barrett-Joyner-Halenda (BJH) model for pore size distribution by the adsorption branch on isotherm.

4. Electrocatalytic experiments

The electrochemical station (References 3000, Gamry Instruments, USA) with a

rotating disk electrode (RDE) system were used to conducted the electrochemical measurements. For the preparation of working electrode, the samples were initially ultrasonically dispersed into aqueous inks with the concentration of 2 mg mL^{-1}. 20 μl of the catalyst ink was droped onto a pre-prepared RDE with the diamerter of 5 mm and dried at ambient condition, then 5 μl of 0.5 wt. % Nafion aqueous solution was added to increase the adherence. An Ag/AgCl/KCl (3.5 M) electrode and a platinum wire was selected as the reference and counter electrodes, the volume of 100 mL electrolyte was added into a 5-port electrolytic cell with N_2 gas inlet during the tests. The HER tests were performed in1 M KOH while HzOR in 1 M KOH with 0.5 M N_2H_4. All the electrochemical data were treated with iR correction except for stability tests.

In the direct N_2H_4/H_2O_2 fuel cell (DHHPFC), the catalysts were loaded onto carbon paper (1 cm by 2 cm, 1 mg cm^{-2}, Sigracet 29BC), the anodes were the RuPd/C and commercial 20 wt.% Pt/C catalysts, and their cathodes were all 20 wt.% Pt/C. When testing the DHHPFCs, 5 M H_2O_2 in 0.5 M H_2SO_4 as the catholyte and 1 M N_2H_4 in 4 M KOH as the anolyte were flowed into the cell compartments with a flow rate of 5 mL min^{-1} by a two-channel peristaltic pump (EC200-01, Gaoss Union) connected with the silicone tube. The Nafion N115 membrane was used as the proton exchange membrane to separate two compartments.

5. Computational Method and Details

In this work, due to the computational resource restraints, the small-size models of Pd_{28} and Ru_{28} clusters were selected, and Pd atoms were disordered doped on Ru clusters in the ratio of 2:8, and the alloy RuPd model was obtained. The geometric structures of intermediates and transition states were optimized using either a restricted or unrestricted Perdew-Burke-Ernzerhof (PBE) exchange-correlation functional implemented in DMol^3.[1–4] The DFT-based relativistic semi-core pseudopotential (DSPP) and double numerical plus *d*-functions (DND) basis sets were used to calculate the energy of structural optimization and transition state search. The reaction pathway of the H_2O decomposition was calculated using the combination of a linear synchronous transit (LST) and quadratic synchronous transit (QST) algorithm with conjugated gradient optimization method. The convergence criterion of the geometric optimization was set to be 1.0×10^{-5} hartree for energy change, 2.0×10^{-3} hartree/Å for the gradient, and 3.0×10^{-3} Å for the displacement, respectively. The convergence criterion of the frequency calculation was set to be 1.0×10^{-7} hartree for energy change, 1.0×10^{-3} hartree/Å for the gradient, and 3.0×10^{-3} Å for the displacement, respectively. The smearing parameter was set to be 0.001 Hartree in geometric optimization.

The adsorption energies were calculated by by the equations (1)-(3):

$$E_{a\text{-}H2O}=E_{H2O*}-E_{*}-E_{H2O} \quad (1)$$

$$E_{a\text{-}H}=E_{(H*)}-E_{*}-1/2E_{H2} \quad (2)$$

$$E_{a\text{-}OH}=E_{OH*}-E_{*}-(E_{H2O}-1/2E_{H2}) \quad (3)$$

E_{H2O*} denote the total electronic energy of adsorbed H_2O system on the Ru/RuPd/Pd, E_{*} denote the total electronic energy of Ru/RuPd/Pd, E_{H2} and E_{H2O} denote the total electronic energy of H_2 and H_2O.

The reactions from N_2H_4 to N_2 on the Ru, RuPd or Pd are (4)-(9):

$$N_2H_4+*\rightarrow N_2H_4* \quad (4)$$

$$N_2H_4*\rightarrow N_2H_3*+H^++e^- \quad (5)$$

$$N_2H_3*\rightarrow N_2H_2*+H^++e^- \quad (6)$$

$$N_2H_2*\rightarrow N_2H*+H^++e^- \quad (7)$$

$$N_2H*\rightarrow N_2*+H^++e^- \quad (8)$$

$$N_2*\rightarrow N_2+* \quad (9)$$

The relative free energy of the dischargeing reaction from N_2H_4 to N_2 on the Ru, RuPd or Pd were calculated by the equations (10)-(15):

$$\Delta G_1 = G_{N2H4*} - G_* + G_{N2H4} \quad (10)$$

$$\Delta G_2 = G_{N2H3*} + 1/2G_{H2} - G_{N2H4*} \quad (11)$$

$$\Delta G_3 = G_{N2H2*} + 1/2G_{H2} - G_{N2H3*} \quad (12)$$

$$\Delta G_4 = G_{N2H*} + 1/2G_{H2} - G_{N2H2*} \quad (13)$$

$$\Delta G_5 = G_{N2*} + 1/2G_{H2} - G_{N2H*} \quad (14)$$

$$\Delta G_6 = G_{N2*} - G_* + G_{N2} \quad (15)$$

The Gibbs free energy (G) can be calculated from follow formula (16), the ZPE and TS could be obtained from the calculation of vibrational frequencies for the adsorbed species, T is temperature (298.15 K).

$$G = E + ZPE - TS \quad (16)$$

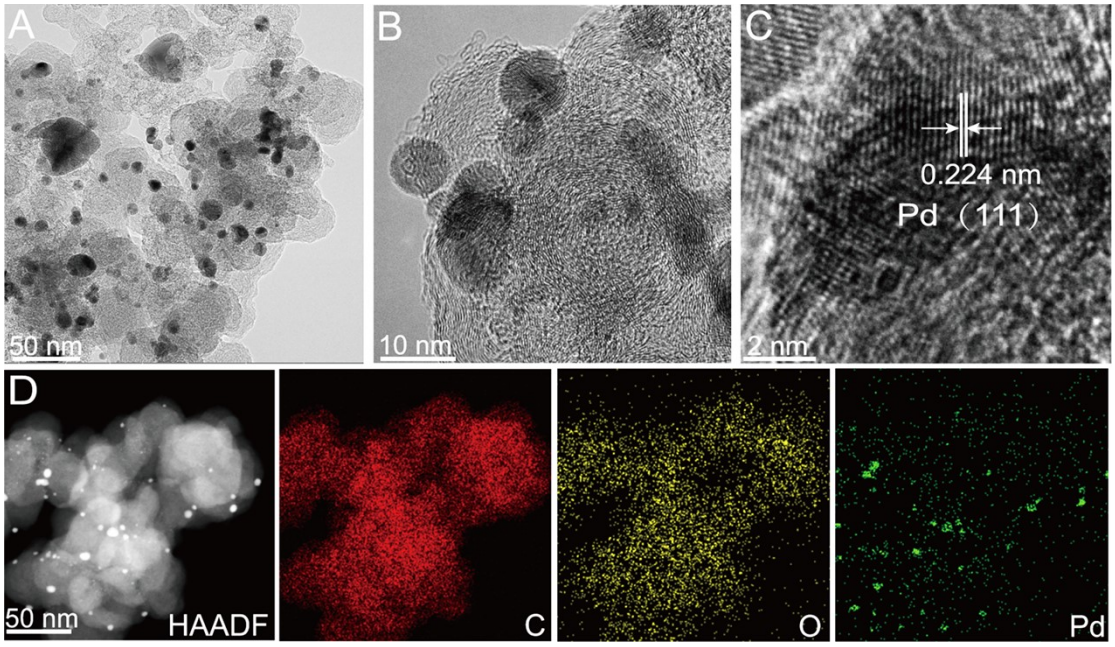

Figure S1 (A-C) TEM images at different magnifications of Pd/C and (D) TEM HAADF and elemental mapping images of C, O and Pd of Pd/C.

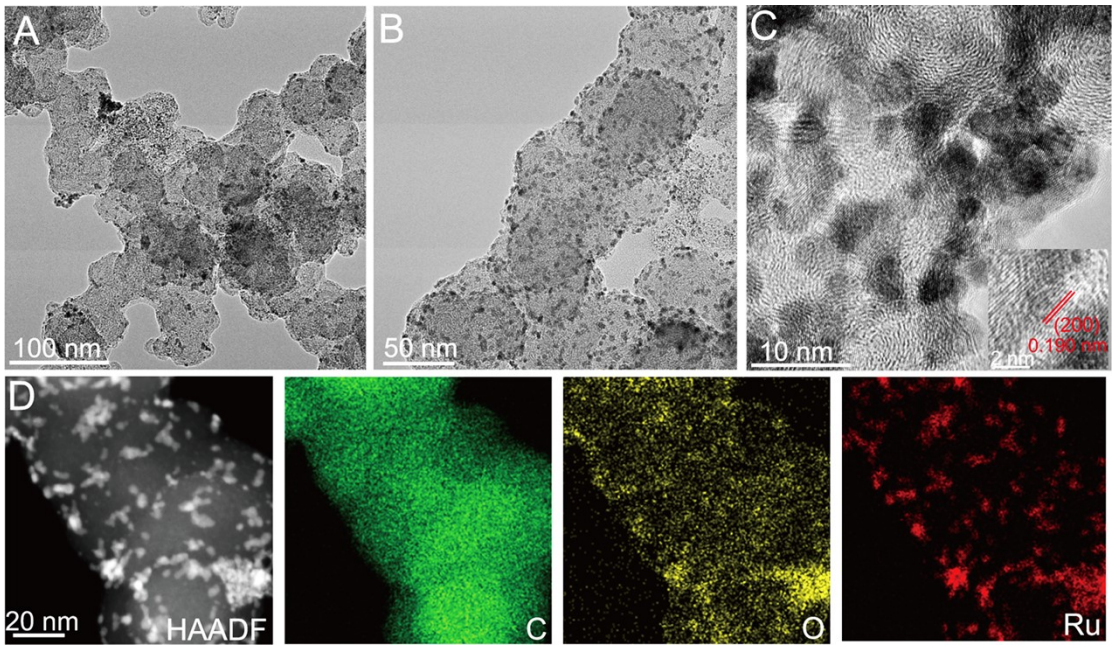

Figure S2 (A-C) TEM images at different magnifications of Ru/C and (D) TEM HAADF and elemental mapping images of C, O and Ru of Ru/C.

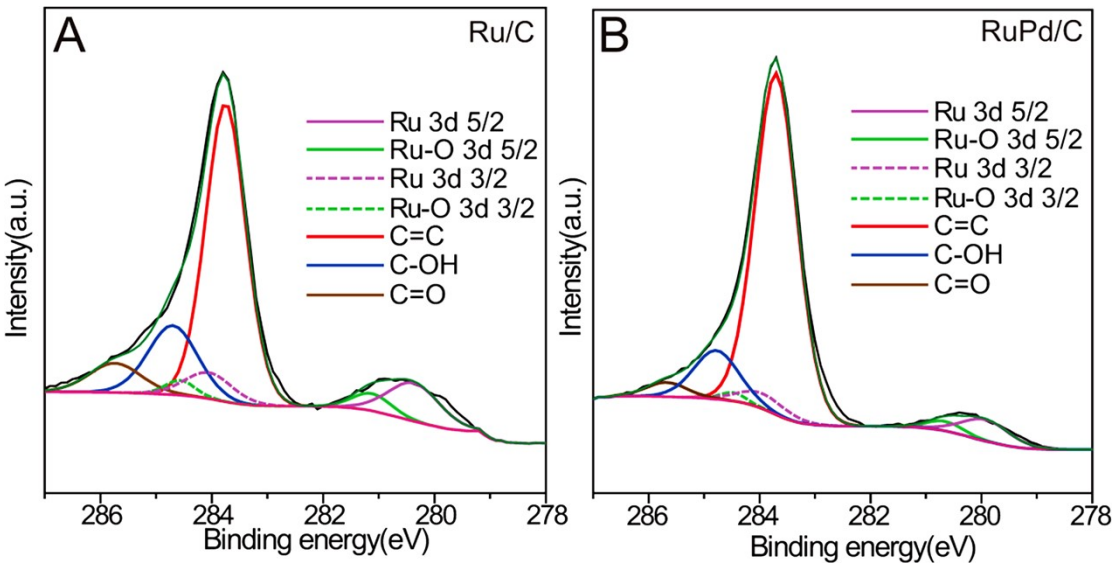

Figure S3 XPS spectroscopic analysis of Ru 3d in Ru/C and RuPd/C.

For Ru/C, the high-resolution XPS regions of Ru 3d overlap with C 1s, the peaks at 280.4 and 281.1 eV correspond to Ru $3d_{5/2}$,and Ru-O $3d_{5/2}$, combined with Ru $3d_{3/2}$ peak located at 284.1 eV and Ru-O $3d_{3/2}$ peak at 284.6 eV, meanwhile, the peaks at 283.8, 284.7 and 285.7 eV are attributed to C=C, C-OH and C=O moieties, respectively.

For RuPd/C, the peaks at 279.9 and 280.7 eV correspond to Ru $3d_{5/2}$, and Ru-O $3d_{5/2}$, combined with Ru $3d_{3/2}$ peak located at 284.0 eV and Ru-O $3d_{3/2}$ peak at 284.5 eV, meanwhile, the peaks at 283.7, 284.8 and 285.7 eV are attributed to C=C, C-OH and C=O moieties, respectively.

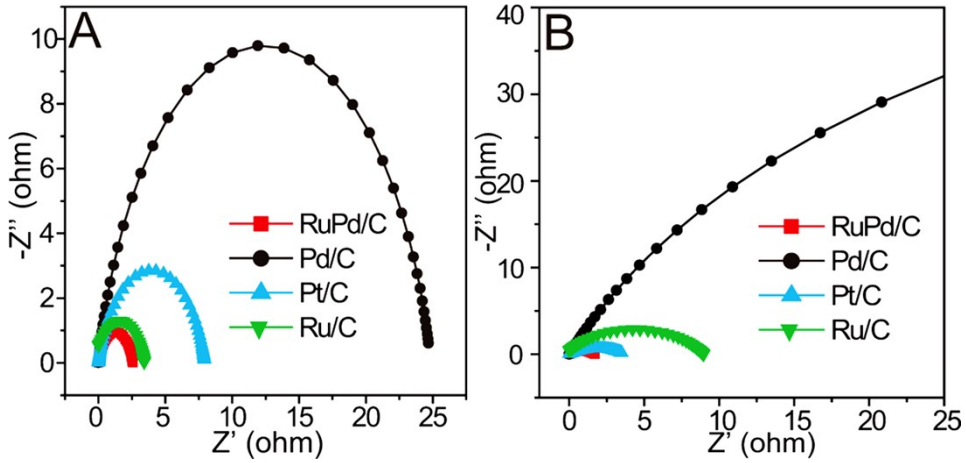

Figure S4 (A) The electrochemical impedance spectra of (A) HER in 1 M KOH and HzOR in 1 M KOH+0.5 M N_2H_4.

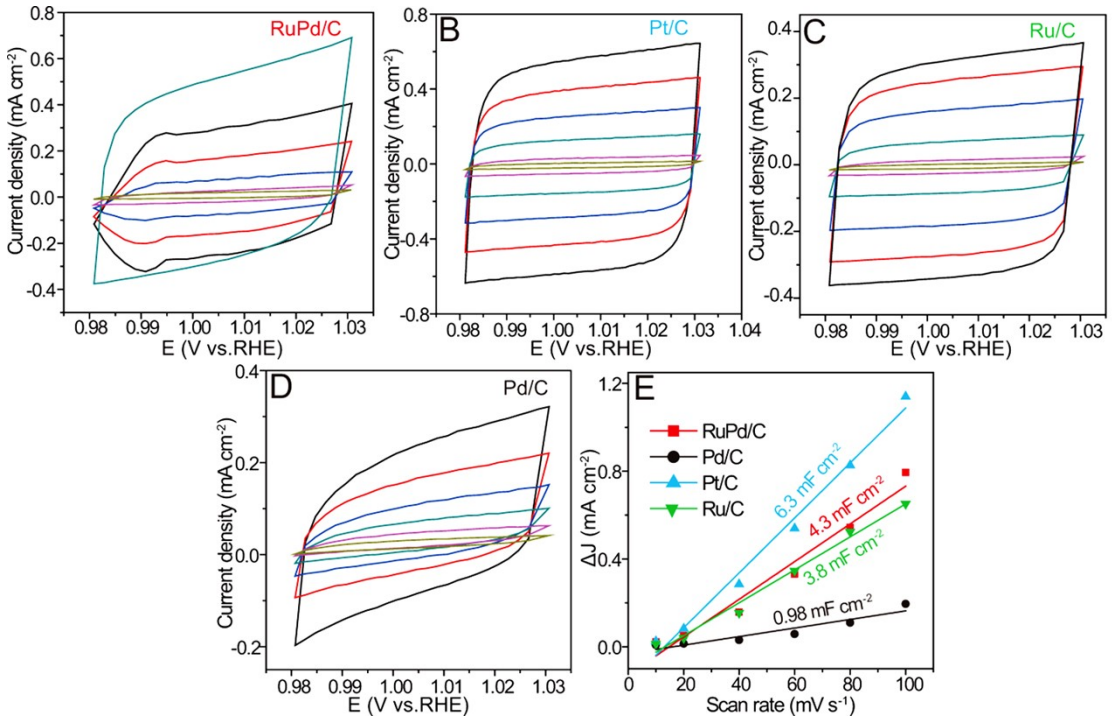

Figure S5 CV curves at different scan rates (20, 40, 60, 80 and 100 mV s^{-1}) of (A) RuPd/C, (B) Pt/C, (C) Ru/C and (D) Pd/C, (E) the calculated C_{dl} values based on the corresponding difference in the current density at 1.005 V plotted against scan rates.

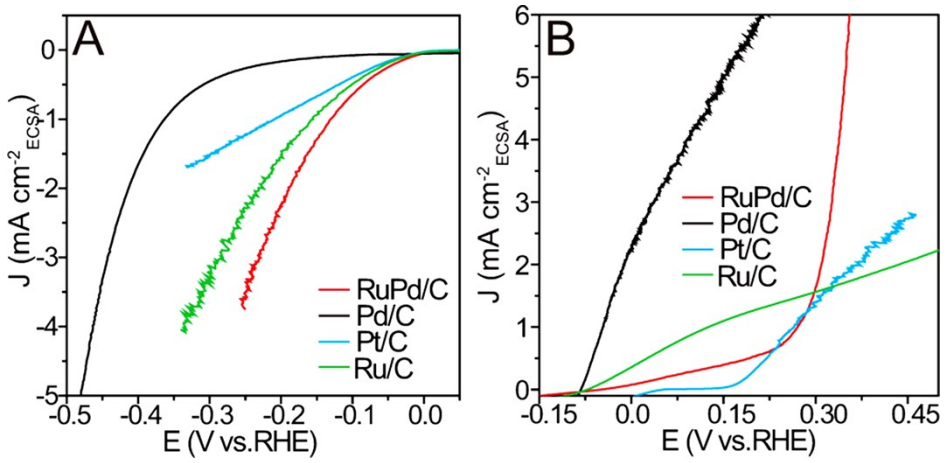

Figure S6 The ESCA-normalized LSV curves of (A) HER and (B) HzOR.

ECSA was calculated based on the equation: ECSA = C_{dl}/C_s, where C_{dl} is general specific capacitance, C_s value was generally found to be in the range of 20-60 μF cm^{-2} and the capacitance of 40 μF cm^{-2} was used to calculate the ECSA, which is roughly considered equal to the specific surface area.[5-9]

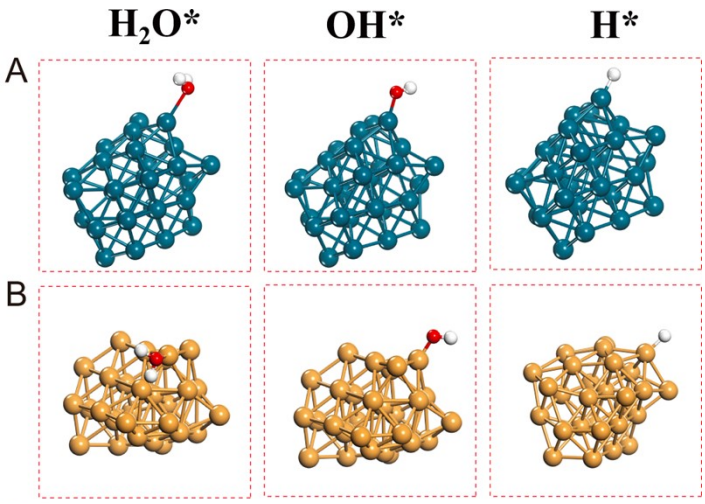

Figure S7 Structural models of H_2O*, OH* and H* adsorbed on (A) pure Pd and (B) pure Ru. The blue, yellow, red and white stands for Pd, Ru, O and H atom, respectively.

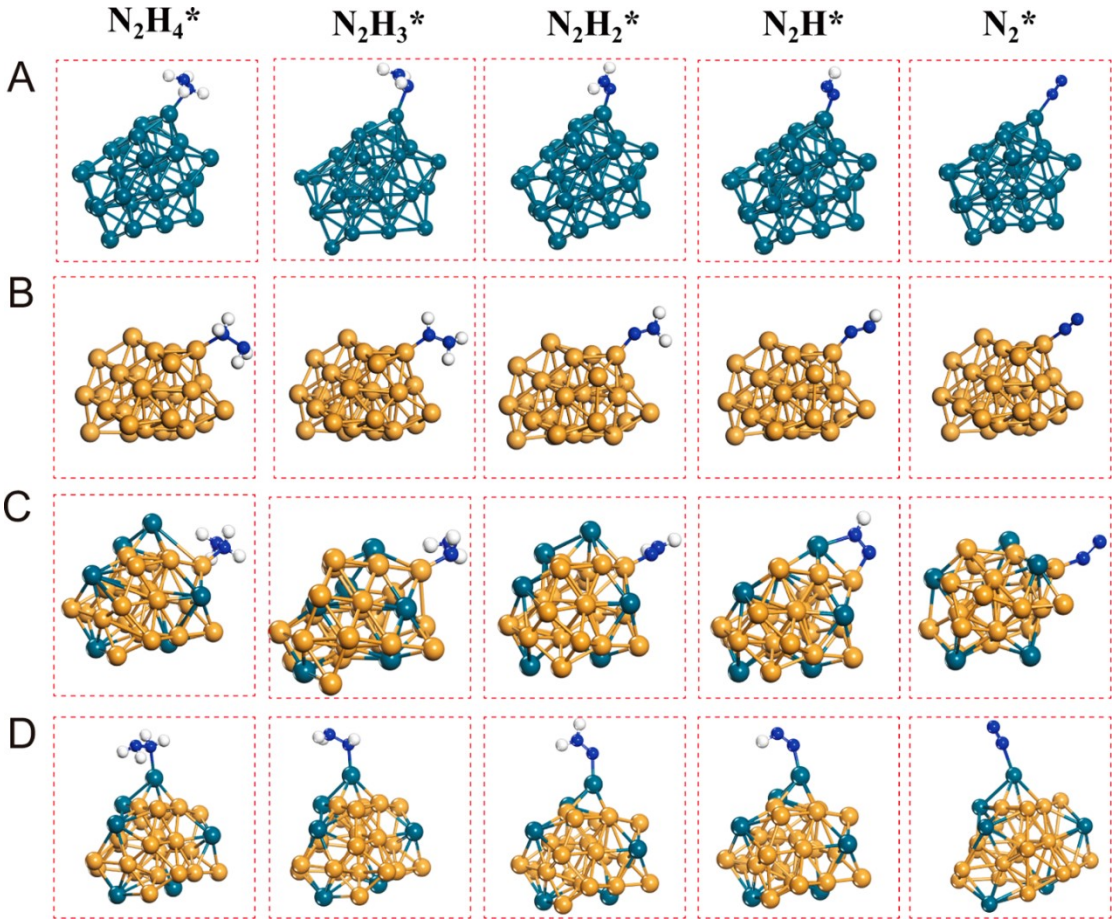

Figure S8 Structural models of reaction intermediates adsorbed on the (A) pure Pd, (B) pure Ru, (C) RuPd (Ru site) and (D) RuPd (Pd site) for stepwise N_2H_4 dehydrogenation.

Table S1. The BET surface area, pore volume and pore diameter of different samples.

Samples	BET surface area (m^2 /g)	Pore volume (cm^3 /g)	Pore diameter (nm)
RuPd/C	160.41	0.31	12.41
Ru/C	178.59	0.43	13.71
Pd/C	176.85	0.50	14.86

Table S2. Quantitative XPS information of different samples.

Samples	Ru (at%)			Pd (at%)			C (at%)	O (at%)
	total Ru	Ru	Ru-O	Total Pd	Pd	Pd-O		
RuPd/C	1.57	1.15	0.42	0.40	0.18	0.22	87.00	6.47
Pd/C				1.84	1.40	0.44	90.15	8.01
Ru/C	1.89	1.50	0.39				84.85	8.58

Table S3 Comparison on the activity of the recently reported HzOR catalysts in alkaline electrolyte.

Catalysts	Electrolyte	Potential @10 mA cm^{-2} (mV)	Potential @100 mA cm^{-2} (mV)	Tafel slope (mV dec^{-1})	References
Ru/PNC	1.0 M KOH + 0.5 M N_2H_4	-77.9	-49.1	37.2	This work
Pt/C	1.0 M KOH + 0.5 M N_2H_4	165.7	233.6	59.9	This work
Cu_1Pd_3/C	1.0 M KOH + 0.5 M N_2H_4	560	--	58	J. Mater Sci Technol 2023, 143, 20-29
CC@WO_3/Ru-450	1.0 M KOH + 0.5 M N_2H_4	-58	18	--	Chem. Eng. J. 2022, 430, 132953
Ru/MPNC	1.0 M KOH + 0.5 M N_2H_4	-39	--	40	Nano Energy 2022, 100, 107467
RhIr MNs	1.0 M KOH + 0.5 M N_2H_4	-12	117	30	J. Mater. Chem. A, 2021, 9, 18323-18328
Mo-Ni_3N/Ni/NF	1.0 M KOH + 0.1 M N_2H_4	-0.3	50	48	Adv. Funct. Mater. 2021, 31, 2103673
$CoSe_2$/NF	1.0 M KOH + 0.5 M N_2H_4	-17	170	--	Angew. Chem. Int. Ed. 2018, 57, 7649-7653
$RhRu_{0.5}$ alloy	1.0 M KOH + 1.0 M N_2H_4	-48	54	47.6	Adv. Mater. 2023, DOI:10.1002/adma.202301533.
Ru/PNC	1.0 M KOH + 0.5 M N_2H_4	-20.4	72.3	52.8	Appl Catal B-Environ 2023, 323, 122145
Rh/N-CBs	1.0 M KOH + 0.05 M N_2H_4	72	--	38.3	ACS Appl. Mater. Interfaces 2019, 11, 35039-35049
Cu_1Ni_2-N	1.0 M KOH + 0.5 M N_2H_4	0.5	25	44.1	Adv. Energy Mater. 2019, 1900390
MoO_2/Co–NF	1.0 M KOH + 0.5 M N_2H_4	-73	-21	22.9	J. Mater. Chem. A, 2022, 10, 17297-17306
NiCo@C/MXene/CF	1.0 M KOH + 0.5 M N_2H_4	-96	-25	75	Nat. Commun. 2021, 12, 4182
Ir/PNC	1.0 M KOH + 0.5 M N_2H_4	16.7	--	46.6	Chem. Commun. 2022, 58, 2347
Ru_{40}@mONC	1.0 M KOH + 0.5 M N_2H_4	-53	8	25	Nano. Res. 2022, 15, 5134-5142
V-Ni_3N NS	1.0 M KOH + 0.1 M N_2H_4	2	46	31	ACS Appl. Mater. Interfaces 2021, 13, 3881−3890
Rh-NSs-300	1.0 M KOH + 0.5 M N_2H_4	-103	--	15.4	Chem. Eng. J. 2023, 463, 142385
PW-Co_3N	1.0 M KOH + 0.1 M N_2H_4	-55	-10	14	Nat. Commun. 2020, 11, 1853

Ni_2P/Zn–Ni–P-0.1	1.0 M KOH + 0.1 M N_2H_4	27	--	33	J. Mater. Chem. A, 2023, 11, 2191
RhPb NFs	1.0 M KOH + 0.1 M N_2H_4	18	175	44	Chem. Eng. J. 2022, 440, 135848
Ni_3N-Co_3NPNAs/ NF	1.0 M KOH + 0.1 M N_2H_4	-88	--	21.6	Angew. Chem. Int. Ed. 2021, 60, 5984–5993
NiCo-$MoNi_4$ HMNAs/NF	1.0 M KOH + 0.1 M N_2H_4	-30	--	28.5	Chem. Eng. J. 2021, 414, 128818
CC@WS_2/Ru -450	1.0 M KOH + 0.5 M N_2H_4	-74	--	42.2	Adv. Funct. Mater. 2022, 32, 2109439
Ni(Cu) CNPs	1.0 M KOH + 0.5 M N_2H_4	-18	76	--	J. Mater. Chem. A 2020, 8, 21084–21093

References

(1) Perdew, J. P.; Burke, K.; Ernzerhof, M. Generalized Gradient Approximation Made Simple. *J. Phys. Rev. Lett.* **1996**, *77*, 3865−3868.

(2) Delley, B. An All-Electron Numerical Method for Solving the Local Density Functional for Polyatomic Molecules. *J. Chem. Phys.* **1990**, *92*, 508−517.

(3) Delley, B. From Molecules to Solids with the Approach. *J. Chem. Phys.* **2000**, *113*, 7756−7764.

(4) Tal, J.; Perdew, J. P.; Staroverov, V. N. Physical Content of the Exact Kohn-Sham Orbital Energies: Band Gaps and Derivative Discontinuities. *Phys. Rev.* **1983**, *51*, 1884.

(5) Kibsgaard, J.; Tsai, C.; Chan, K.; Benck, J. D.; Nørskov, J. K.; Abild-Pedersen, F.; Jaramillo, T. F. Designing an Improved Transition Metal Phosphide Catalyst for Hydrogen Evolution Using Experimental and Theoretical Trends. *Energy Environ. Sci.* **2015**, *8*, 3022–3029.

(6) Kibsgaard, J.; Chen, Z.; Reinecke, B. N.; Jaramillo, T. F. Engineering the Surface Structure of MoS_2 to Preferentially Expose Active Edge Sites for Electrocatalysis. *Nat. Mater.* **2012**, *11*, 963–969.

(7) Li, D. J.; Maiti, U. N.; Lim, J.; Choi, D. S.; Lee, W. J.; Oh, Y.; Lee, G. Y.; Kim, S. O. Molybdenum Sulfide/N-Doped CNT Forest Hybrid Catalysts for High-Performance Hydrogen Evolution Reaction. *Nano Lett.* **2014**, *14*, 1228–1233.

(8) Li J.; Zhou Q.; Zhong C.; Li S.; Shen Z.; Pu J.; Liu J.;, Zhou Y.; Zhang H.; Ma H. $(Co/Fe)_4O_4$ Cubane-Containing Nanorings Fabricated by Phosphorylating Cobalt Ferrite for Highly Efficient Oxygen Evolution Reaction. *ACS Catal.* **2019**, *9*, 3878-3887.

(9 Li J.; Zhang C.; Zhang C.; Ma H.; Yang Y.; Guo Z.; Wang Y.; Ma H. Electronic Configuration of Single Ruthenium Atom Immobilized in Urchin-Like Tungsten Trioxide towards Hydrazine Oxidation-Assisted Hydrogen Evolution under Wide pH Media. *Chem. Eng. J.* **2022**, *430*, 132953.